



TransCom N₂O model
inter-comparison

R. L. Thompson et al.

This discussion paper is/has been under review for the journal Atmospheric Chemistry and Physics (ACP). Please refer to the corresponding final paper in ACP if available.

TransCom N₂O model inter-comparison, Part II: Atmospheric inversion estimates of N₂O emissions

R. L. Thompson^{1,2}, K. Ishijima³, E. Saikawa^{4,5}, M. Corazza⁶, U. Karstens⁷,
P. K. Patra³, P. Bergamaschi⁶, F. Chevallier², E. Dlugokencky⁸, R. G. Prinn⁴,
R. F. Weiss⁹, S. O'Doherty¹⁰, P. J. Fraser¹¹, L. P. Steele¹¹, P. B. Krummel¹¹,
A. Vermeulen¹², Y. Tohjima¹³, A. Jordan⁷, L. Haszpra^{14,15}, M. Steinbacher¹⁶,
S. Van der Laan¹⁷, T. Aalto¹⁸, F. Meinhardt¹⁹, M. E. Popa^{7,20}, J. Moncrieff²¹, and
P. Bousquet²

¹Norwegian Institute for Air Research, Kjeller, Norway

²Laboratoire des Sciences du Climat et l'Environnement, Gif sur Yvette, France

³Research Institute for Global Change, JAMSTEC, Yokohama, Japan

⁴Center for Global Change Science, MIT, Cambridge, MA, USA

⁵Emory University, Atlanta, GA, USA

⁶Institute for Environment and Sustainability, JRC, Ispra, Italy

⁷Max Planck Institute for Biogeochemistry, Jena, Germany

⁸NOAA Earth System Research Laboratory, Global Monitoring Division, Boulder, CO, USA

⁹Scripps Institution of Oceanography, La Jolla, CA, USA

Title Page

Abstract

Introduction

Conclusions

References

Tables

Figures

◀

▶

◀

▶

Back

Close

Full Screen / Esc

Printer-friendly Version

Interactive Discussion



¹⁰Atmospheric Chemistry Research Group, School of Chemistry, University of Bristol, Bristol, UK

¹¹Centre for Australian Weather and Climate Research, CSIRO, Marine and Atmospheric Research, Aspendale, Victoria, Australia

¹²Energy Research Centre of the Netherlands (ECN), Petten, the Netherlands

¹³National Institute for Environmental Studies, Tsukuba, Japan

¹⁴Hungarian Meteorological Service, Budapest, Hungary

¹⁵Geodetic and Geophysical Institute, Research Centre for Astronomy and Earth Sciences, Hungarian Academy of Sciences, Sopron, Hungary

¹⁶Swiss Federal Laboratories for Materials Science and Technology (Empa), Duebendorf, Switzerland

¹⁷University of Groningen, Groningen, the Netherlands

¹⁸Finnish Meteorological Institute, Helsinki, Finland

¹⁹Umweltbundesamt, Messstelle Schauinsland, Kirchzarten, Germany

²⁰University of Utrecht, Utrecht, the Netherlands

²¹University of Edinburgh, Edinburgh, UK

Received: 15 November 2013 – Accepted: 5 February 2014 – Published: 27 February 2014

Correspondence to: R. L. Thompson (rona.thompson@nilu.no)

Published by Copernicus Publications on behalf of the European Geosciences Union.

ACPD

14, 5271–5321, 2014

TransCom N₂O model inter-comparison

R. L. Thompson et al.

Title Page

Abstract

Introduction

Conclusions

References

Tables

Figures

◀

▶

◀

▶

Back

Close

Full Screen / Esc

Printer-friendly Version

Interactive Discussion



Abstract

This study examines N₂O emission estimates from 5 different atmospheric inversion frameworks. The 5 frameworks differ in the choice of atmospheric transport model, meteorological data, prior uncertainties and inversion method but use the same prior emissions and observation dataset. The mean emissions for 2006 to 2008 are compared in terms of the spatial distribution and seasonality. Overall, there is a good agreement among the inversions for the mean global total emission, which ranges from 16.1 to 18.7 Tg N yr⁻¹ and is consistent with previous estimates. Ocean emissions represent between 31 % and 38 % of the global total compared to widely varying previous estimates of 24 % to 38 %. Emissions from the northern mid to high latitudes are likely to be more important, with a consistent shift in emissions from the tropics and subtropics to the mid to high latitudes in the Northern Hemisphere; the emission ratio for 0–30° N to 30–90° N ranges from 1.5 to 1.9 compared with 2.9 to 3.0 in previous estimates. The largest discrepancies across inversions are seen for the regions of South and East Asia and for tropical and South America owing to the poor observational constraint for these areas and to considerable differences in the modelled transport, especially inter-hemispheric exchange rates and tropical convection. Estimates of the seasonal cycle in N₂O emissions are also sensitive to errors in modelled stratosphere-to-troposphere transport in the tropics and southern extra-tropics. Overall, the results show a convergence in the global and regional emissions compared to previous independent studies.

1 Introduction

Nitrous oxide (N₂O) currently has the third largest contribution to anthropogenic radiative forcing after CO₂ and CH₄, accounting for 0.16 W m⁻² additional forcing since 1750 (Forster et al., 2007). Furthermore, N₂O plays an important role in stratospheric ozone loss and currently the ozone-depleting-potential weighted emissions of N₂O are thought to be the highest of any ozone-depleting substance (Ravishankara et al.,

ACPD

14, 5271–5321, 2014

TransCom N₂O model inter-comparison

R. L. Thompson et al.

Title Page

Abstract

Introduction

Conclusions

References

Tables

Figures

◀

▶

◀

▶

Back

Close

Full Screen / Esc

Printer-friendly Version

Interactive Discussion



TransCom N₂O model
inter-comparison

R. L. Thompson et al.

2009). The atmospheric mole fraction of N₂O has increased significantly since the mid-20th century largely as a result of agricultural activities and, in particular, the use of nitrogen fertilizers (Park et al., 2012). Currently, agricultural emissions from fertilizer use and manure management (4.3–5.8 Tg Nyr⁻¹) and emissions from natural soils (6–7 Tg Nyr⁻¹) account for 60–70 % of global N₂O emissions (Syakila and Kroeze, 2011; Zaehle et al., 2011). The remaining 30–40 % of emissions is from oceans (4.5 Tg Nyr⁻¹) (Duce et al., 2008) and, to a smaller extent, from fuel combustion, industry (Olivier et al., 2005) and biomass burning (together 1.7 Tg Nyr⁻¹) (van der Werf et al., 2010).

N₂O is dominantly produced by microbial processes in soils, sediments and water bodies, specifically, by nitrification and denitrification. Although a lot is already known about these processes from laboratory studies under controlled conditions and in-situ chamber flux measurements, up-scaling to emissions on national or regional scales is hampered by the strongly variable nature of soil fluxes. N₂O production in soils is dependent on a multitude of environmental factors such as soil moisture and temperature, soil type, among others, which interact in complex ways, which are difficult to predict (Butterbach-Bahl and Dannenmann, 2011). In agricultural soils, the type of nitrogen fertilizer and the timing of its application are also important considerations for estimating N₂O emissions. In natural soils, there is a natural nitrogen turnover leading to N₂O emissions but these may be enhanced by the input of reactive nitrogen from fertilizers and other anthropogenic sources by atmospheric transport, erosion, and leaching, leading to so-called indirect anthropogenic emissions (Galloway et al., 2003).

An alternative and complementary approach to up-scaling small-scale fluxes and processes to estimate regional and global N₂O budgets, is to use a top-down approach. Atmospheric inversion is one such top-down approach and uses observations of N₂O mole fractions with a model of atmospheric transport and chemistry in a statistically rigorous way to constrain surface fluxes. This approach has been used previously for estimating N₂O emissions on regional (Corazza et al., 2011; Thompson et al., 2011b) and global scales (Hirsch et al., 2006; Huang et al., 2008; Kort et al., 2011; Prinn et al., 1990; Saikawa et al., 2013; Thompson et al., 2014a). One major advantage of the at-

[Title Page](#)[Abstract](#)[Introduction](#)[Conclusions](#)[References](#)[Tables](#)[Figures](#)[◀](#)[▶](#)[◀](#)[▶](#)[Back](#)[Close](#)[Full Screen / Esc](#)[Printer-friendly Version](#)[Interactive Discussion](#)

This paper is divided into four main sections. In Sect. 2, we outline the inversion frameworks and CTMs, as well as the prior flux estimates and atmospheric observations used in this study. Section 3.1 presents a validation of the inversion results by comparing the mole fractions simulated using the posterior fluxes with observations while Sect. 3.2 analyses the spatial and temporal distribution of the posterior fluxes. In Sect. 3.3, we compare these estimates with those of previous studies and conclude with a discussion of the major challenges for estimating N₂O emissions from atmospheric inversions.

2 Methods

2.1 Inversion frameworks

Five different inversion frameworks participated in Part II of this experiment. In this paper, we refer to each of the frameworks according to the CTM used followed by “-I” to indicate that this is the inversion framework. Although the frameworks may be used with a different CTM, in this study the naming is unambiguous as a different CTM was used with each one (see Table 1). All frameworks use the Bayesian inversion method to find the optimal surface fluxes, that is, the fluxes that provide the best fit to the atmospheric observations, \mathbf{y} , while being guided by the prior flux estimates, \mathbf{x}_b , and their uncertainties (for details about the Bayesian method refer to Tarantola, 2005). Based on Bayesian theory, and Gaussian-error hypotheses, the optimal fluxes are those that minimize the cost function:

$$J(\mathbf{x}) = (\mathbf{x} - \mathbf{x}_b)^T \mathbf{B}^{-1} (\mathbf{x} - \mathbf{x}_b) + (H(\mathbf{x}) - \mathbf{y})^T \mathbf{R}^{-1} (H(\mathbf{x}) - \mathbf{y}) \quad (1)$$

where the prior flux uncertainties are described by the error covariance matrix, \mathbf{B} , the observation uncertainties are described by the error covariance matrix, \mathbf{R} , and H is an operator of the atmospheric transport and chemistry as defined by the CTM in each inversion framework. Depending on the inversion framework, H is either a matrix or

Title Page

Abstract

Introduction

Conclusions

References

Tables

Figures

◀

▶

◀

▶

Back

Close

Full Screen / Esc

Printer-friendly Version

Interactive Discussion



model performance can be directly applied in this study when considering differences between posterior fluxes. All inversions were run for the period 2005–2009 but only output from 2006 onwards was analysed as 2005 was used as a spin-up year. Also, when presenting mean emission results, the years 2006–2008 are used, as the end of 2009 is not as well constrained in the inversions. In addition to the 1 yr spin-up all models started with their best initial conditions estimates established after previous longer integrations of the CTMs.

2.2.1 Stratospheric N₂O loss

Loss of N₂O in the stratosphere through photolysis (circa 90% of the loss, Minshwaner et al., 1993) and reaction with O(¹D) (circa 10%) was calculated in each model in every grid-cell and time-step. Although the exact photolysis and oxidation rates varied between models (according to the CTM used to calculate the photolysis rate and O(¹D) concentration) these were scaled such that the global annual total loss of N₂O was approximately 12.5 TgN, consistent with estimates of the atmospheric abundance and the lifetime of N₂O, which is estimated to be between 124 and 130 yr (Prather et al., 2012; Volk et al., 1997).

2.2.2 Prior fluxes

The prior N₂O flux was comprised from estimates of the different sources, that is, from soils (including both natural and agricultural soils), ocean, biomass burning, waste, fuel combustion and industry (see Table 3). For soil fluxes, we used the terrestrial biosphere model, O-CN (Zaehle and Friend, 2010), which is driven by reconstructed observed climate (CRU-NCEP, Climate Research Unit – National Centre for Environmental Prediction), N-fertiliser application, and atmospheric N-deposition data and provides inter-annually varying estimates at monthly and 3.75° × 2.5° (longitude by latitude) resolution as described in Zaehle et al. (2011). For the ocean flux, we used the Pelagic Interaction Scheme for Carbon and Ecosystem Studies (PISCES) ocean

Title Page

Abstract

Introduction

Conclusions

References

Tables

Figures

◀

▶

◀

▶

Back

Close

Full Screen / Esc

Printer-friendly Version

Interactive Discussion



biogeochemistry model (Dutreuil et al., 2009), which provides inter-annually varying fluxes at monthly and $1.0^\circ \times 1.0^\circ$ resolution. For waste, fuel combustion, and industrial emissions, we used EDGAR-4.1 (Emission Database for Greenhouse gas and Atmospheric Research, available at: <http://edgar.jrc.ec.europa.eu/index.php>), which are estimated for the reference year 2005 and were provided annually at $1.0^\circ \times 1.0^\circ$ resolution. Biomass burning estimates from GFED-2.1 (Global Fire Emissions Database) (van der Werf et al., 2010) were used, which were provided monthly and at $1.0^\circ \times 1.0^\circ$ resolution. In total, the global emission for 2005 to 2009 was 16.8, 16.3, 16.8, 16.2 and 16.4 Tg Nyr^{-1} , respectively.

2.2.3 Degrees of freedom

The number of degrees of freedom in the inversion is an important factor for determining how closely the posterior fluxes resemble the prior ones. For MOZART4-I and ACTMt42I67-I, which solve the inversion using coarse regions, the number of degrees of freedom is substantially reduced representing a strong constraint on the inversion as only the mean flux in each region is optimized and the flux pattern within each region remains as described a priori. On the other hand, solving for fine regions i.e. at the resolution of the transport model, as in TM5-I, TM3-I and LMDZ4-I, benefits from additional regularization constraints, such as spatial correlations of the prior flux errors (used in the definition of **B**). For TM5-I the spatial correlation length (200 km) means that the grid cells are only weakly correlated to one another resulting in a weak constraint, whereas in LMDZ4-I, longer scale lengths are used (500 km for land and 1000 km for ocean) resulting in a stronger constraint (see Table 2).

2.3 Atmospheric observations

Atmospheric observations of N_2O mole fractions (nmolmol^{-1} equivalently parts-per-billion, abbreviated as ppb) were pooled from two global networks, NOAA CCGG (Carbon Cycle and Greenhouse Gases) and AGAGE (Advanced Global Atmospheric

Title Page

Abstract

Introduction

Conclusions

References

Tables

Figures

◀

▶

◀

▶

Back

Close

Full Screen / Esc

Printer-friendly Version

Interactive Discussion



Gases Experiment), as well as from a number of smaller regional networks and independent stations (see Fig. 1 and Table 4). From the NOAA CCGG network, 42 sites were included. Approximately weekly discrete air samples are taken at these sites, which are subsequently analysed for N₂O using GC-ECD (Gas Chromatography Electron Capture Detector). These data are reported on the NOAA-2006A calibration scale (Hall et al., 2007) and have a reproducibility of 0.4 ppb based on the mean difference of flask pairs. The AGAGE network consists of 5 in-situ GC-ECD instruments. These data are reported on the SIO-1998 scale and have a reproducibility of approximately 0.1 ppb (Prinn et al., 2000). The MPI-BGC (Max Planck Institute for Biogeochemistry) network consists of 3 sites for discrete air samples and 2 sites with in-situ GC-ECD instruments. These data are also reported on the NOAA-2006A scale and have a reproducibility of about 0.3 ppb. In addition, data from 9 independently run stations with in-situ GC-ECD instruments were included (see Table 4).

These stations do not all use the same calibration scale and, thus, offsets exist between the measurements. Furthermore, even in the case where the measurements are reported on the same scale, there still may be offsets owing to systematic errors. These offsets can introduce significant errors in the optimized fluxes if they are not accounted for prior to, or in, the inversion. For this reason, calibration offsets were estimated using inter-calibration data for each of the in-situ stations, and for the 3 MPI-BGC flask sites together, relative to the NOAA-2006A scale (see Table 5). Since the inter-calibration data were not complete for all times and all sites, the offsets were included into the optimization problem in inversion frameworks with this capacity (i.e. in LMDZ4-I and TM5-I, and only TM5-I resolves the offsets temporally using annual resolution). In this case, the best estimates of the offsets were used as prior values. In the case that they could not be optimized (i.e. in MOZART4-I, ACMTt42167-I, and TM3-I) the given values were used to correct the observations prior to the inversion.

**TransCom N₂O model
inter-comparison**

R. L. Thompson et al.

Title Page

Abstract

Introduction

Conclusions

References

Tables

Figures

I◀

▶I

◀

▶

Back

Close

Full Screen / Esc

Printer-friendly Version

Interactive Discussion



3 Results and discussion

3.1 Validation with atmospheric observations

3.1.1 Meridional gradients

Meridional gradients are some of the most commonly used observational parameters to assess CTMs, as they provide a constraint on features such as inter-hemispheric transport and latitudinal flux distributions (Gloor et al., 2007; Patra et al., 2011). Figure 2 shows the observed annual mean meridional gradient (2006 to 2009) compared with simulations by each CTM integrated with the corresponding posterior fluxes. The gradients were calculated from detrended and deseasonalized N₂O mole fractions at background surface sites. A very good agreement was found with the observed gradient at the surface (correlation coefficient $R^2 \geq 0.9$). In MOZART4-I, the mean mole fraction is approximately 1.5 ppb higher, which is most likely due to too high mole fractions in the initial conditions (see also Fig. A1), but it still captures the gradient reasonably well.

Gradients in the pressure-weighted column mean N₂O were also compared against observations from HIPPO (Hiaper Pole-to-Pole Observations, <http://hippo.ucar.edu>) campaigns in January and November 2009 (Fig. 3). In contrast to the surface, the simulations all underestimate the total column inter-hemispheric gradient in January by about 1 ppb (circa 50%). In November, the inter-hemispheric gradient is smaller and is matched more closely by the models; however, there is an overall offset of about 1 ppb (except MOZART4-I where its 1.5 ppb offset compensates). The offset in November may be in part due to a calibration difference between HIPPO and the NOAA data, which were used in the inversion, as comparisons of the HIPPO data between 0 and 2000 m around 19° N and 14° S with the NOAA data at Mauna Loa (19.5° N, 155.6° W) and Samoa (14.3° S, 170.6° E), respectively, show an offset of about 0.5 ppb. The underestimate of the gradient in January may be due to the models underestimating N₂O mole fractions in the upper troposphere as the agreement with the observed column is

TransCom N₂O model inter-comparison

R. L. Thompson et al.

Title Page

Abstract

Introduction

Conclusions

References

Tables

Figures

◀

▶

◀

▶

Back

Close

Full Screen / Esc

Printer-friendly Version

Interactive Discussion



prior flux estimate with no terrestrial biosphere seasonal cycle (see Part I, Thompson et al., 2014b) suggesting that the reason for the too early minimum was not related to transport problems but rather to the seasonality in the fluxes. This also seems to be the case for MOZART4-I and TM3-I, which have the smallest shift in the seasonal cycle relative to the prior fluxes (this is discussed in more detail in Sect. 3.2.3). At MLO, all CTMs simulate a too early minimum, as was also the case a priori, but the amplitude a posteriori is closer to that observed. The timing of the minimum, in April, in the models is consistent with the expected maximum influence of stratospheric air in the troposphere owing to the downward branch of the Brewer Dobson circulation, which has a maximum in December to February in the NH. However, the fact that the observed minimum occurs later may suggest that the influence of STT is overestimated in the models and/or that the seasonality is still not correct in the fluxes at this latitude.

For the Southern Hemisphere sites, SMO and CGO, all models agree well with the observed seasonal cycles except MOZART4-I at SMO and TM3-I at CGO. At SPO, however, all models underestimate the amplitude and MOZART-I and TM3-I are also out of phase. It has been shown with N₂O isotope measurements that the seasonality at CGO is determined by the combined influences of STT and ocean fluxes leading to the observed minimum in April (Park et al., 2012). With the a priori fluxes, both TM3-I and LMDZ4-I had the phase of the seasonal cycle at CGO out by nearly 6 months indicating a problem with STT in the Southern Hemisphere (see Thompson et al., 2014b). A similar error in MOZART4-I was observed at SPO as well. However, a posteriori, LMDZ4-I has a much-improved fit to the phase at CGO and SPO, which was achieved by increasing the amplitude of the flux seasonality in the Southern Ocean, whereas TM3-I and MOZART4-I make nearly no adjustment (this is discussed further in Sect. 3.2.3).

3.2 Comparison of posterior emissions

In this section, we present a comparison of the posterior emission estimates. All posterior emissions were compared after they were interpolated from the corresponding model grid to 1° × 1° resolution.

3.2.1 Global means

Table 6 shows the global total emission a priori and the global total emission and sink a posteriori calculated by each inversion framework. On the basis of the posterior emissions, the inversions can be grouped into two categories: (1) those with generally low global totals, i.e. MOZART4-I, ACTMt32167-I and TM3-I and (2) those with high global totals, i.e. TM5-I and LMDZ4-I, where low and high are defined relative to the prior. This categorisation also corresponds to how the observations were assimilated in the inversion; the first category inversions assimilate monthly (MOZART4-I and ACTMt32167-I) or weekly (TM3-I) means, while those in the second category (TM5-I and LMDZ4-I) use the atmospheric data at their sampled time. This feature of the category 2 inversions means that they are also sensitive to the synoptic variability of the observations, while in the category 1 inversions this signal is smoothed-out. MOZART4-1 and ACTMt32167-1, which have the lowest global total estimates, also differ from the other inversions in that they solve for emissions in large regions as opposed to solving the emissions at the resolution of the transport model. Another reason for the low posterior global totals in MOZART4-I (the lowest of all inversions) is that the N₂O mole fractions are overestimated in the initial conditions, which results in the emissions being underestimated and a too low atmospheric N₂O growth rate (see Fig. A3). For this reason, the MOZART-I estimates are not included further in the flux totals. All inversion frameworks had very similar global total sinks, within less than 1 TgNyr⁻¹ of each other for each year, thus differences in the calculated loss rate is not a reason for the differences in global total emissions.

Overall the global distribution of N₂O emissions was similar in all inversions and close to that a priori (Fig. 5). The highest emissions were found in the subtropical and tropical regions of South America, Africa and Asia, in Europe and the eastern states of the USA. However, the inversions differ in the relative importance of emissions in each of these sub-continental regions. Figure 6 shows the annual mean flux increments made by each inversion, i.e. the mean posterior minus prior flux. There are a number of fea-

Title Page

Abstract

Introduction

Conclusions

References

Tables

Figures

◀

▶

◀

▶

Back

Close

Full Screen / Esc

Printer-friendly Version

Interactive Discussion



tures in the increments that are common to all inversions: (1) lower (relative to the prior) emissions in temperate land regions in the SH, (2) higher emissions in central Europe, (3) higher emissions in central Africa and (4) no significant change in northern Eurasia and Canada. On the other hand, the inversions differ significantly in the direction and/or magnitude of the flux increments for the USA (eastern states), South and East Asia, and tropical South America. This information is summarized in Fig. 7, which shows the median absolute deviation (MAD) of the annual mean emissions from all 5 inversions. Regions with highest MAD correspond to regions with the greatest discrepancy among the inversions.

To better examine the differences between the a posteriori emissions, we compare the annual mean zonally integrated emissions plotted against latitude and the accumulated emissions from south to north (Fig. 8). By plotting the emissions in this way, differences in the latitudinal distribution of the emissions are more apparent and may be assessed in terms of different features of the CTMs used in the inversions, such as the rate of inter-hemispheric and vertical mixing. Moving from south to north, one can see that all inversions estimate lower emissions compared to the prior in the Southern Hemisphere; it is only north of the Equator that some of the inversions have a higher accumulated emission. TM5-I has the highest emission estimate for the Southern Hemisphere tropics and is also the most southern crossing point with the prior accumulated emissions. This is likely related to the fact that TM5-I has a long inter-hemispheric exchange time (1.7 yr compared to the observed 1.4 yr in 2006, based on SF₆ mole fractions at BRW, MLO, CGO and SPO (Patra et al., 2011)), which would mean that in order to match the observed atmospheric N₂O mole fraction in the Southern Hemisphere tropics, higher emissions in this region are required. At circa 30° N, LMDZ4-I surpasses both the prior and TM5-I accumulated emissions owing to very large emission estimates in the Northern Hemisphere sub-tropics. LMDZ4-I (in the present 19-layer configuration) has a relatively short inter-hemispheric exchange time, 1.2 yr in 2006 (Patra et al., 2011), and has been found to have a very diffusive PBL in the Northern Hemisphere mid latitudes (Geels et al., 2007). These features likely lead to too

**TransCom N₂O model
inter-comparison**

R. L. Thompson et al.

Title Page

Abstract

Introduction

Conclusions

References

Tables

Figures

◀

▶

◀

▶

Back

Close

Full Screen / Esc

Printer-friendly Version

Interactive Discussion



high emissions in the NH sub-tropics and mid latitudes. North of circa 50° N, the zonally integrated emission differs very little among the inversions and the prior, however, the accumulated total emission at 90° N differs owing to the aforementioned disparities.

3.2.2 Regional means

Figure 9 shows the annual mean total emissions for 7 sub-continental and 3 ocean regions from each of the inversions and the prior, in addition, the corresponding range, median, and MAD of the emissions are given in Table 7. For only 3 out of the 7 land regions is there a significant change in emissions with respect to the prior. Here, we define significant to mean that: (1) all inversions agree on the direction of the change and (2) the prior value is outside the range of the posterior median and MAD. These regions are Africa, Europe and Australasia. For Australasia, the contribution to the global total (2 %, median posterior value) and the absolute change relative to the prior (0.08 TgNyr⁻¹) are very small, and thus this region is not discussed further. Europe was found to have 30 % (0.24 TgNyr⁻¹) higher emissions than estimated a priori and contributes on average 6 % (median posterior value) to the global total emission. Africa was also found to have higher emissions relative to the prior (by 10 %, equivalent to 0.29 TgNyr⁻¹) and contributes on average 20 % to the global total emission. Of the regions where the change was not considered significant, North America as well as South and Tropical America still satisfied the second criterion. For North America, all inversions except LMDZ4-I estimated lower emissions (by 26 %, equivalent to 0.26 TgNyr⁻¹) bringing its contribution to the global total to 4 %, and for South and Tropical America, all inversions except TM5-I estimate lower emissions (by 9 %, equivalent to 0.22 TgNyr⁻¹) bringing its contribution to the global total to 14 %. For South Asia and North Asia, however, the inversions differed significantly both in the direction of change as well as in the magnitude. While the total emission from North Asia is small (2 % of the global) that from South Asia is very important (approximately 17 % of the global).

There are several reasons why the inversions differ so substantially for South Asia. First, this region is not well covered by the observation network. Emissions from this

Title Page

Abstract

Introduction

Conclusions

References

Tables

Figures

◀

▶

◀

▶

Back

Close

Full Screen / Esc

Printer-friendly Version

Interactive Discussion



TransCom N₂O model inter-comparison

R. L. Thompson et al.

Title Page

Abstract

Introduction

Conclusions

References

Tables

Figures

◀

▶

◀

▶

Back

Close

Full Screen / Esc

Printer-friendly Version

Interactive Discussion



region are only constrained by the 2 in-situ sites, HAT and COI, and by the discrete sampling sites, BKT, GMI, LLN, and TAP. Second, since the prior flux uncertainties are calculated proportionally to the prior flux, the prior uncertainty for this region is large allowing the inversions considerable freedom to adjust the fluxes here. Lastly, differences in the modelled transport, such as the tropical convection, monsoon flow, and shifts in the North Pacific storm track, which are important in determining outflow from the Asian continent (Stohl et al., 2002) may also contribute to the disparity among emission estimates for South Asia. Stohl et al. (2002) showed that tracers emitted in Asia south of 30° N, particularly in India, are readily transported toward the ITCZ and thus could be one reason why LMDZ4-I, with a fast inter-hemispheric mixing rate, predicts the highest emissions for South Asia. Similar reasoning also applies to the large discrepancy for South and Tropical America. South and Tropical America is very poorly covered by the observation network (see Fig. 1) and the prior flux uncertainty for this region is very large. The posterior emission estimates for this region are also likely to be sensitive to features of the modelled transport, in particular, convective transport.

Unlike for the land regions, there is reasonably good agreement among inversions for the ocean regions. All ocean regions satisfy the second criterion, and only the region 30° S–30° N does not also satisfy the first criterion. The emissions for the Southern Ocean (90–30° S) were found to be smaller than estimated a priori, contributing 6 % (median posterior value) to the global total, while emissions for the tropical (30° S–30° N) and northern (30–90° N) ocean regions, the emissions were found to be larger, contributing 22 % and 7 % to the global total, respectively.

3.2.3 Seasonal variability

The mean seasonal cycle for each of the 7 land and 3 ocean regions was calculated by averaging the total monthly emissions over the period 2006 to 2008 and is shown in Fig. 10. For the Northern Hemisphere temperate land regions, Europe, North America and North Asia, the prior flux seasonal cycle predicts a late summer maximum, i.e. between July and August. However, all inversions estimate smaller emissions in July

**TransCom N₂O model
inter-comparison**

R. L. Thompson et al.

[Title Page](#)[Abstract](#)[Introduction](#)[Conclusions](#)[References](#)[Tables](#)[Figures](#)[◀](#)[▶](#)[◀](#)[▶](#)[Back](#)[Close](#)[Full Screen / Esc](#)[Printer-friendly Version](#)[Interactive Discussion](#)

For the Southern Hemisphere regions of South and Tropical America and Africa, there is very little seasonality in the prior fluxes. However, all of the inversions estimate a March–April minimum for South and Tropical America and similarly (except LMDZ4-1) for Africa. For South and Tropical America, the March–April minimum is not easy to explain in terms of soil N₂O fluxes. In fact, from the few existing regional measurements of N₂O fluxes in tropical South America only a small seasonal cycle has been observed with elevated fluxes during the wet season from March–May (D’Amelio et al., 2009). Therefore, it is likely that the minimum in the optimized fluxes is due to transport errors since the timing of the atmospheric N₂O minimum in April, determined to a large extent by STT, is not captured by the models, thus to match observations, the inversions estimate lower N₂O emissions at this time. It is possible that the impact of this transport error on the optimized fluxes would not be so strong if there were better observational constraints for South America. The same also applies for Africa where the minimum in March–April cannot be explained in terms of variability in soil fluxes as this time corresponds to the wet season when the highest N₂O emissions are expected.

For the ocean regions, the phase and amplitude of the seasonal cycles a posteriori differ little from that a priori. In the Southern Ocean, the minimum in April and maximum in September–October is consistent with the independent estimate of Nevison et al. (2005) and is largely driven by the upwelling and subsequent venting of subsurface water, which is enriched in N₂O. In the tropical and northern ocean regions, the seasonal cycle is much smaller in amplitude but is also likely driven by seasonal changes in upwelling.

3.3 Comparison with other estimates

To put this study into context with previous work, we compare our results to independent N₂O emission estimates. We have chosen 5 studies, including 2 atmospheric inversions (Hirsch et al., 2006; Huang et al., 2008) and 3 inventory and model-based estimates (Denman et al., 2007; Syakila and Kroeze, 2011; Zaehle et al., 2011), which are global in coverage and include estimates of N₂O emissions from all sources and

**TransCom N₂O model
inter-comparison**

R. L. Thompson et al.

Title Page

Abstract

Introduction

Conclusions

References

Tables

Figures

◀

▶

◀

▶

Back

Close

Full Screen / Esc

Printer-friendly Version

Interactive Discussion



are thus appropriate for this comparison. (The study of Zaehle et al. (2011) is not completely independent as it uses the same terrestrial biosphere model, O-CN, for the estimate of N₂O soil emissions as was used in this study's prior emissions, however, the O-CN simulations used different climate forcing and N-deposition.) Figure 11 compares the global, land, and ocean total emissions, as well as the emission distribution by semi-hemisphere, where available. Although the exact period of each study varies, they all include estimates of the global N₂O budget in the 2000s. At the global scale, all estimates agree within the range of uncertainties (no uncertainty estimate was provided by Syakila and Kroeze (2011)). Progress, however, has been made in reducing the level of uncertainty from 4.5 TgNyr⁻¹ in the IPCC AR4 (Intergovernmental Panel on Climate Change Fourth Assessment Report, 2007) to 0.7 TgNyr⁻¹ in this study (1σ, 68 % probability assuming Gaussian error distribution) with the complete range of inversions from 16.1 to 18.7 TgNyr⁻¹. Previous studies differ in the apportionment between land and ocean emissions, with ocean estimates varying from 24 % to 38 % of the global total, whereas we found fairly good agreement among the inversions participating in this study with ocean estimates varying between 31 % and 38 % of the global total. At the semi-hemisphere scale, we find a few important differences between our median estimates and previous ones: for the region 90° S to 30° S we estimate higher emissions (7 % of the global total), for the region 0° to 30° N we estimate lower emissions (41 %), and for 30° N to 90° N slightly higher emissions (23 %). Comparing the ratio for emissions in the regions 0° to 30° N and 30° N to 90° N, all our inversions give a lower value (from 1.5 to 1.9) compared with 3.0 (Hirsch et al., 2006) and 2.9 (Huang et al., 2008) for the periods 1998–2005 and 2001–2005, respectively. Since our estimates are for a later period (2006–2008), this difference may reflect real changes in emissions. It is known that emissions have been increasing in Asia, particularly, in China, over the past decade, which has also increased the overall emission in the region 30° N to 90° N, while no significant trends have been found in other regions (Thompson et al., 2014a). The increase in China has primarily been driven by

an increase in N-fertilizer usage and to a lesser extent, an increase in industrial and combustion sources of N₂O (Thompson et al., 2014a).

4 Summary and conclusions

In this study we have compared the N₂O emission estimates of 5 inversion frameworks and analysed these in terms of their spatial distribution and seasonal variability. In general, there is a high level of agreement among the 5 inversions participating in this study despite the differences in inversion approach, atmospheric transport model and meteorological data used. This gives us confidence that there has been substantial progress made in terms of uncertainty reduction. Moreover, we have identified emission patterns that are robust, that is, common to all inversion frameworks as well as those that depend strongly on the modelled transport and/or inversion set-up. The salient results are summarized as follows:

- the mean global annual N₂O emission ranges between 16.1 and 18.7 with a median and MAD of 16.7 and 0.7 TgNyr⁻¹, respectively for the years 2006 to 2008;
- ocean emissions were found to contribute between 31 % and 38 % and land emissions between 62 % and 69 % to the global total;
- the apportionment of emissions to each semi-hemisphere was fairly close among inversions, with 7 ± 1 % to 90–30° S, 28 ± 2 % to 30–0°, 41 ± 1 % to 0–30° N and 23 ± 1 % to 30–90° N (median and MAD as a percentage of the global total), thus making the Northern Hemisphere tropics and subtropics the most important latitudinal range for N₂O emissions globally;
- all inversions estimated lower emissions for the latitudes 90–30° S relative to the prior, however, the median estimate (7 % of the global total) was still higher than that found in previous studies (0 to 4 %);

TransCom N₂O model inter-comparison

R. L. Thompson et al.

Title Page

Abstract

Introduction

Conclusions

References

Tables

Figures

◀

▶

◀

▶

Back

Close

Full Screen / Esc

Printer-friendly Version

Interactive Discussion



TransCom N₂O model inter-comparison

R. L. Thompson et al.

Title Page

Abstract

Introduction

Conclusions

References

Tables

Figures

◀

▶

◀

▶

Back

Close

Full Screen / Esc

Printer-friendly Version

Interactive Discussion



- the ratio of emissions in 0–30° N to 30–90° N is smaller in all inversions (range of 1.52 to 1.91 and median of 1.9) compared to previous studies (2.9 and 3.0), representing a change in the percentage of the global total of –16 % for 0–30° N and of +3 % for 30–90° N;
- 5 – all inversions estimated higher emissions in Europe and Africa relative to the prior, contributing 6 % ($1.04 \pm 0.20 \text{ TgNyr}^{-1}$) and 20 % ($3.36 \pm 0.04 \text{ TgNyr}^{-1}$) (median and MAD values), respectively to the global total compared with 5 % (0.80 TgNyr^{-1}) and 18 % (3.07 TgNyr^{-1}) a priori;
- all inversions (except LMDZ4) estimate lower emissions in North America contributing 4 % ($0.74 \pm 0.11 \text{ TgNyr}^{-1}$) (median values) to the global total compared to 6 % (1.00 TgNyr^{-1}) a priori;
- all inversions (except TM5) estimate lower emissions in South and Tropical America contributing 14 % ($2.33 \pm 0.27 \text{ TgNyr}^{-1}$) to the global total compared to 15 % (2.55 TgNyr^{-1}) a priori;
- 15 – the largest uncertainties were found in the estimates for South and Tropical America and South Asia owing to uncertainties in the modelled atmospheric transport and to the poor observational constraint for these regions.

In general, the global N₂O budget, the total emissions and their spatial distribution, are close to what has been found from previous studies. One notable difference in our inversion estimates compared to previous ones though, is the shift in the distribution in the Northern Hemisphere, with lower emissions in the tropics and subtropics and higher emissions in temperate latitudes. Moreover, our inversions show a convergence of estimates both at the global and sub-continental scale. This good agreement is most likely due to the expansion of the atmospheric observation network. However, considerable uncertainties remain, especially in the less well-constrained regions of South Asia and South and Tropical America. These regions also appear to be very sensitive to uncertainties in the modelled atmospheric transport. Also sensitive to atmospheric transport,

TransCom N₂O model inter-comparison

R. L. Thompson et al.

Title Page

Abstract

Introduction

Conclusions

References

Tables

Figures

◀

▶

◀

▶

Back

Close

Full Screen / Esc

Printer-friendly Version

Interactive Discussion



is the seasonal flux variability. Although this appears to be robust in the northern extra-tropics, for the tropics and southern extra-tropics, this is strongly dependent on having adequate representation of the timing of the maximum in STT and in vertical mixing, which is still not the case in most CTMs. However, inter-annual variations in fluxes are likely to be more robust as the year-to-year variations in STT are not as great as the seasonal variations. Improvements in the accuracy of N₂O emission estimates from atmospheric inversions, and to move towards emissions monitoring in the context of the Kyoto Protocol, would require improvements to modelling of atmospheric transport, in particular, STT, which has a very strong influence on tropospheric N₂O mole fractions.

Acknowledgements. We would like to thank S. Zaehle, L. Bopp, and G. van der Werf for providing their N₂O emissions estimates. We also thank E. Kort and S. Wofsy for the use of the HIPPO data. Additionally, we would like to acknowledge everyone who contributes to the ongoing measurement of N₂O in all networks without which we would not have been able to make this inter-comparison study.

References

- Butterbach-Bahl, K. and Dannenmann, M.: Denitrification and associated soil N₂O emissions due to agricultural activities in a changing climate, *Curr. Opin. Environ. Sustain.*, 3, 389–395, 2011.
- Butterbach-Bahl, K., Baggs, E. M., Dannenmann, M., Kiese, R., and Zechmeister-Boltenstern, S.: Nitrous oxide emissions from soils: how well do we understand the processes and their controls?, *Philos. T. Roy. Soc. B*, 368, 1621, doi:10.1098/rstb.2013.0122, 2013.
- Chevallier, F., Fisher, M., Peylin, P., Serrar, S., Bousquet, P., Bréon, F.-M., Chédin, A., and Ciais, P.: Inferring CO₂ sources and sinks from satellite observations: method and application to TOVS data, *J. Geophys. Res.*, 110, D24309, doi:10.1029/2005JD006390, 2005.
- Corazza, M., Bergamaschi, P., Vermeulen, A. T., Aalto, T., Haszpra, L., Meinhardt, F., O'Doherty, S., Thompson, R., Moncrieff, J., Popa, E., Steinbacher, M., Jordan, A., Dlugokencky, E., Brühl, C., Krol, M., and Dentener, F.: Inverse modelling of European N₂O emis-

**TransCom N₂O model
inter-comparison**

R. L. Thompson et al.

Title Page

Abstract

Introduction

Conclusions

References

Tables

Figures

◀

▶

◀

▶

Back

Close

Full Screen / Esc

Printer-friendly Version

Interactive Discussion



sions: assimilating observations from different networks, *Atmos. Chem. Phys.*, 11, 2381–2398, doi:10.5194/acp-11-2381-2011, 2011.

Courtier, P., Thépaut, J. N., and Hollingsworth, A.: A strategy for operational implementation of 4-D-Var, using an incremental approach, *Q. J. Roy. Meteor. Soc.*, 120, 1367–1387, 1994.

5 D'Amelio, M. T. S., Gatti, L. V., Miller, J. B., and Tans, P.: Regional N₂O fluxes in Amazonia derived from aircraft vertical profiles, *Atmos. Chem. Phys.*, 9, 8785–8797, doi:10.5194/acp-9-8785-2009, 2009.

Denman, K. L., Brasseur, G. P., Chidthaisong, A., Ciais, P., Cox, P. M., Dickinson, R. E., Hauglustaine, D., Heinze, C., Holland, E., Jacob, D., Lohmann, U., Ramachandran, S., da Silva Dias, P. L., Wofsy, S. C., and Zhang, X.: Couplings between changes in the climate system and biogeochemistry, in: *Climate Change 2007: the Physical Science Basis, Contribution of Working Group I to the Fourth Assessment Report of the Intergovernmental Panel on Climate Change*, edited by: Solomon, S. D., Qin, D., Manning, M., Chen, Z., Marquis, M., Averyt, K. B., Tignor, M., and Miller, H. L., Cambridge University Press, Cambridge, 499–587, 2007.

15 Duce, R. A., LaRoche, J., Altieri, K., Arrigo, K. R., Baker, A. R., Capone, D. G., Cornell, S., Dentener, F., Galloway, J., Ganeshram, R. S., Geider, R. J., Jickells, T., Kuypers, M. M., Langlois, R., Liss, P. S., Liu, S. M., Middelburg, J. J., Moore, C. M., Nickovic, S., Oeschies, A., Pedersen, T., Prospero, J., Schlitzer, R., Seitzinger, S., Sorensen, L. L., Uematsu, M., Ulloa, O., Voss, M., Ward, B., and Zamora, L.: Impacts of atmospheric anthropogenic nitrogen on the open ocean, *Science*, 320, 893–897, 2008.

Dutreuil, S., Bopp, L., and Tagliabue, A.: Impact of enhanced vertical mixing on marine biogeochemistry: lessons for geo-engineering and natural variability, *Biogeosciences*, 6, 901–912, doi:10.5194/bg-6-901-2009, 2009.

25 Forster, P., Ramaswamy, V., Artaxo, P., Berntsen, T., Betts, R., Fahey, D. W., Haywood, J., Lean, J., Lowe, D. C., Myhre, G., Nganga, J., Prinn, R., Raga, G., Schultz, M., and Van Dorland, R.: Changes in atmospheric constituents and in radiative forcing, in: *Climate Change 2007: the Physical Science Basis, Contribution of Working Group I to the Fourth Assessment Report of the Intergovernmental Panel on Climate Change*, edited by: Solomon, S., Qin, D., Manning, M., Chen, Z., Marquis, M., Averyt, K. B., Tignor, M., and Miller, H. L., Cambridge University Press, Cambridge, UK, 2007.

30 Galloway, J. N., Aber, J., Erisman, J. W., Seitzinger, S. P., Howarth, R. W., Cowling, E. B., and Cosby, B. J.: The nitrogen cascade, *Bioscience*, 53, 341–356, 2003.

TransCom N₂O model inter-comparison

R. L. Thompson et al.

Title Page

Abstract

Introduction

Conclusions

References

Tables

Figures

◀

▶

◀

▶

Back

Close

Full Screen / Esc

Printer-friendly Version

Interactive Discussion



Geels, C., Gloor, M., Ciais, P., Bousquet, P., Peylin, P., Vermeulen, A. T., Dargaville, R., Aalto, T., Brandt, J., Christensen, J. H., Frohn, L. M., Haszpra, L., Karstens, U., Rödenbeck, C., Ramonet, M., Carboni, G., and Santaguida, R.: Comparing atmospheric transport models for future regional inversions over Europe – Part 1: mapping the atmospheric CO₂ signals, *Atmos. Chem. Phys.*, 7, 3461–3479, doi:10.5194/acp-7-3461-2007, 2007.

Gloor, M., Dlugokencky, E., Brenninkmeijer, C., Horowitz, L., Hurst, D. F., Dutton, G., Crevoisier, C., Machida, T., and Tans, P.: Three-dimensional SF₆ data and tropospheric transport simulations: signals, modeling accuracy, and implications for inverse modeling, *J. Geophys. Res.*, 112, D15112, doi:10.1029/2006jd007973, 2007.

Hall, B. D., Dutton, G. S., and Elkins, J. W.: The NOAA nitrous oxide standard scale for atmospheric observations, *J. Geophys. Res.*, 112, D09305, doi:10.1029/2006jd007954, 2007.

Hirsch, A. I., Michalak, A. M., Bruhwiler, L. M., Peters, W., Dlugokencky, E. J., and Tans, P. P.: Inverse modeling estimates of the global nitrous oxide surface flux from 1998–2001, *Global Biogeochem. Cy.*, 20, GB1008, doi:10.1029/2004gb002443, 2006.

Huang, J., Golombek, A., Prinn, R., Weiss, R., Fraser, P., Simmonds, P., Dlugokencky, E. J., Hall, B., Elkins, J., Steele, P., Langenfelds, R., Krummel, P., Dutton, P., and Porter, L.: Estimation of regional emissions of nitrous oxide from 1997 to 2005 using multinet network measurements, a chemical transport model, and an inverse method, *J. Geophys. Res.*, 113, D17313, doi:10.1029/2007JD009381, 2008.

Kort, E. A., Patra, P. K., Ishijima, K., Daube, B. C., Jimenez, R., Elkins, J., Hurst, D., Moore, F. L., Sweeney, C., and Wofsy, S. C.: Tropospheric distribution and variability of N₂O: evidence for strong tropical emissions, *Geophys. Res. Lett.*, 38, L15806, doi:10.1029/2011gl047612, 2011.

Lin, S., Iqbal, J., Hu, R., and Feng, M.: N₂O emissions from different land uses in mid-subtropical China, *Agr. Ecosyst. Environ.*, 136, 40–48, doi:10.1016/j.agee.2009.11.005, 2010.

Minschwaner, K., Salawitch, R. J., and McElroy, M. B.: Absorption of solar radiation by O₂: implications for O₃ and lifetimes of N₂O, CFCl₃, and CF₂Cl₂, *J. Geophys. Res.*, 98, 10543–10561, 1993.

Nevison, C. D., Keeling, R. F., Weiss, R. F., Popp, B. N., Jin, X., Fraser, P. J., Porter, L. W., and Hess, P. G.: Southern Ocean ventilation inferred from seasonal cycles of atmospheric N₂O and O₂/N₂ at Cape Grim, Tasmania, *Tellus B*, 57, 218–229, 2005.

TransCom N₂O model
inter-comparison

R. L. Thompson et al.

Title Page

Abstract

Introduction

Conclusions

References

Tables

Figures

◀

▶

◀

▶

Back

Close

Full Screen / Esc

Printer-friendly Version

Interactive Discussion



- Olivier, J. G. J., Van Aardenne, J. A., Dentener, F., Pagliari, V., Ganzeveld, L. N., and Peters, J. A. H. W.: Recent trends in global greenhouse gas emissions: regional trends 1970–2000 and spatial distribution of key sources in 2000, *Environ. Sci.*, 2, 81–99, doi:10.1080/15693430500400345, 2005.
- 5 Park, S., Croteau, P., Boering, K. A., Etheridge, D. M., Ferretti, D., Fraser, P. J., Kim, K. R., Krummel, P. B., Langenfelds, R. L., van Ommen, T. D., Steele, L. P., and Trudinger, C. M.: Trends and seasonal cycles in the isotopic composition of nitrous oxide since 1940, *Nat. Geosci.*, 5, 261–265, 2012.
- 10 Patra, P. K., Houweling, S., Krol, M., Bousquet, P., Belikov, D., Bergmann, D., Bian, H., Cameron-Smith, P., Chipperfield, M. P., Corbin, K., Fortems-Cheiney, A., Fraser, A., Gloor, E., Hess, P., Ito, A., Kawa, S. R., Law, R. M., Loh, Z., Maksyutov, S., Meng, L., Palmer, P. I., Prinn, R. G., Rigby, M., Saito, R., and Wilson, C.: TransCom model simulations of CH₄ and related species: linking transport, surface flux and chemical loss with CH₄ variability in the troposphere and lower stratosphere, *Atmos. Chem. Phys.*, 11, 12813–12837, doi:10.5194/acp-11-12813-2011, 2011.
- 15 Prather, M. J., Holmes, C. D., and Hsu, J.: Reactive greenhouse gas scenarios: systematic exploration of uncertainties and the role of atmospheric chemistry, *Geophys. Res. Lett.*, 39, L09803, doi:10.1029/2012gl051440, 2012.
- 20 Prinn, R. G., Cunnold, D., Rasmussen, R., Simmonds, P., Alyea, F., Crawford, A., Fraser, P., and Rosen, R.: Atmospheric emissions and trends of nitrous oxide deduced from 10 years of ALE-GAGE data, *J. Geophys. Res.*, 95, 18369–18385, 1990.
- 25 Prinn, R. G., Weiss, R. F., Fraser, P. J., Simmonds, P. G., Cunnold, D. M., Alyea, F. N., O'Doherty, S., Salameh, P., Miller, B. R., Huang, J., Wang, R. H. J., Hartley, D. E., Harth, C., Steele, L. P., Sturrock, G., Midgley, P. M., and McCulloch, A.: A history of chemically and radiatively important gases in air deduced from ALE/GAGE/AGAGE, *J. Geophys. Res.*, 105, 17751–17792, 2000.
- Ravishankara, A. R., Daniel, J. S., and Portmann, R. W.: Nitrous oxide (N₂O): the dominant ozone-depleting substance emitted in the 21st century, *Science*, 326, 123–125, 2009.
- 30 Rayner, P. J., Enting, I. G., Francey, R. J., and Langenfelds, R.: Reconstructing the recent carbon cycle from atmospheric CO₂, δ¹³C and O₂/N₂ observations, *Tellus B*, 51, 213–232, 1999.

TransCom N₂O model
inter-comparison

R. L. Thompson et al.

Title Page

Abstract

Introduction

Conclusions

References

Tables

Figures

◀

▶

◀

▶

Back

Close

Full Screen / Esc

Printer-friendly Version

Interactive Discussion



Rödenbeck, C.: Estimating CO₂ sources and sinks from atmospheric mixing ratio measurements using a global inversion of atmospheric transport, Technical Report, Max Planck Institute for Biogeochemistry, Jena, Germany, 6, 2005.

5 Saikawa, E., Prinn, R. G., Dlugokencky, E., Ishijima, K., Dutton, G. S., Hall, B. D., Langenfelds, R., Tohjima, Y., Machida, T., Manizza, M., Rigby, M., O'Doherty, S., Patra, P. K., Harth, C. M., Weiss, R. F., Krummel, P. B., van der Schoot, M., Fraser, P. B., Steele, L. P., Aoki, S., Nakazawa, T., and Elkins, J. W.: Global and regional emissions estimates for N₂O, Atmos. Chem. Phys. Discuss., 13, 19471–19525, doi:10.5194/acpd-13-19471-2013, 2013.

10 Smith, K. A., Thomson, P. E., Clayton, H., McTaggart, I. P., and Conen, F.: Effects of temperature, water content and nitrogen fertilisation on emissions of nitrous oxide by soils, Atmos. Environ., 32, 3301–3309, 1998.

Stohl, A., Eckhardt, S., Forster, C., James, P., and Spichtinger, N.: On the pathways and timescales of intercontinental air pollution transport, J. Geophys. Res.-Atmos., 107, 4684, doi:10.1029/2001jd001396, 2002.

15 Syakila, A. and Kroeze, C.: The global nitrous oxide budget revisited, Greenhouse Gas Measurement and Management, 1, 17–26, 2011.

Tarantola, A.: Inverse Problem Theory and Methods for Model Parameter Estimation, Society for Industrial and Applied Mathematics, Philadelphia, 2005.

20 Thompson, R. L., Bousquet, P., Chevallier, F., Rayner, P. J., and Ciais, P.: Impact of the atmospheric sink and vertical mixing on nitrous oxide fluxes estimated using inversion methods, J. Geophys. Res., 116, D17, doi:10.1029/2011jd015815, 2011a.

Thompson, R. L., Gerbig, C., and Rödenbeck, C.: A Bayesian inversion estimate of N₂O emissions for western and central Europe and the assessment of aggregation errors, Atmos. Chem. Phys., 11, 3443–3458, doi:10.5194/acp-11-3443-2011, 2011b.

25 Thompson, R. L., Chevallier, F., Crotwell, A. M., Dutton, G., Langenfelds, R. L., Prinn, R. G., Weiss, R. F., Tohjima, Y., Nakazawa, T., Krummel, P. B., Steele, L. P., Fraser, P., O'Doherty, S., Ishijima, K., and Aoki, S.: Nitrous oxide emissions 1999 to 2009 from a global atmospheric inversion, Atmos. Chem. Phys., 14, 1801–1817, doi:10.5194/acp-14-1801-2014, 2014a.

30 Thompson, R. L., Patra, P. K., Ishijima, K., Saikawa, E., Corazza, M., Karstens, U., Wilson, C., Bergamaschi, P., Dlugokencky, E., Sweeney, C., Prinn, R. G., Weiss, R. F., O'Doherty, S., Fraser, P. J., Steele, L. P., Krummel, P. B., Saunio, M., Chipperfield, M., and Bousquet, P.: TransCom N₂O model inter-comparison – Part 1: Assessing the influence of transport and

surface fluxes on tropospheric N₂O variability, *Atmos. Chem. Phys. Discuss.*, 14, 2307–2362, doi:10.5194/acpd-14-2307-2014, 2014b.

van der Werf, G. R., Randerson, J. T., Giglio, L., Collatz, G. J., Mu, M., Kasibhatla, P. S., Morton, D. C., DeFries, R. S., Jin, Y., and van Leeuwen, T. T.: Global fire emissions and the contribution of deforestation, savanna, forest, agricultural, and peat fires (1997–2009), *Atmos. Chem. Phys.*, 10, 11707–11735, doi:10.5194/acp-10-11707-2010, 2010.

Volk, C. M., Elkins, J. W., Fahey, D. W., Dutton, G. S., Gilligan, J. M., Loewenstein, M., Podolske, J. R., Chan, K. R., and Gunson, M. R.: Evaluation of source gas lifetimes from stratospheric observations, *J. Geophys. Res.*, 102, 25543–25564, 1997.

Zaehle, S. and Friend, A. D.: Carbon and nitrogen cycle dynamics in the O-CN land surface model: 1. Model description, site-scale evaluation, and sensitivity to parameter estimates, *Global Biogeochem. Cy.*, 24, GB1005, doi:10.1029/2009gb003521, 2010.

Zaehle, S., Ciais, P., Friend, A. D., and Prieur, V.: Carbon benefits of anthropogenic reactive nitrogen offset by nitrous oxide emissions, *Nat. Geosci.*, 4, 601–605, 2011.

ACPD

14, 5271–5321, 2014

TransCom N₂O model inter-comparison

R. L. Thompson et al.

Title Page

Abstract

Introduction

Conclusions

References

Tables

Figures

◀

▶

◀

▶

Back

Close

Full Screen / Esc

Printer-friendly Version

Interactive Discussion



TransCom N₂O model inter-comparison

R. L. Thompson et al.

Table 1. Overview of the CTMs used in the inversions.

Model	Institute	Resolution spatial	vertical	Top boundary pressure (hPa)	Meteorology
MOZART4	MIT	2.5° × 1.88°	56σ ^a	2	MERRA
ACTMt42I67	Jamstec	2.8° × 2.8°	67σ	0.01	JRA25
TM3	MPI-BGC	5.0° × 3.75°	26η ^b	1	ERA-interim
TM5	JRC	6.0° × 4.0°	25η	0.5	ERA-interim
LMDZ4	LSCE	3.75° × 2.5°	19η	4	ERA-interim

^a σ refers to the sigma terrain-following vertical coordinate system.

^b η refers to the eta coordinate system that smoothly transitions from the sigma coordinate near the surface to a pressure coordinate in the stratosphere.

Title Page

Abstract

Introduction

Conclusions

References

Tables

Figures

◀

▶

◀

▶

Back

Close

Full Screen / Esc

Printer-friendly Version

Interactive Discussion



TransCom N₂O model inter-comparison

R. L. Thompson et al.

Table 2. Overview of the inversion frameworks.

Model	Resolution		Inversion method	Scale length in B (km)	
	spatial	temporal		land	ocean
MOZART4 ^a	13 regions	monthly	Analytical	none	none
ACTMt42I67 ^b	22 regions ^f	monthly	Analytical	11 regions	11 regions
TM3 ^c	5.0° × 3.75°	monthly	Variational	500	500
TM5 ^d	6.0° × 4.0°	monthly	Variational	200	200
LMDZ4 ^e	3.75° × 2.5°	monthly	Variational	500	1000

^a Saikawa et al. (2013)

^b based on Rayner et al. (1999)

^c Rödenbeck (2005)

^d Corazza et al. (2011)

^e Thompson et al. (2011a)

^f TransCom-3 regions

Title Page

Abstract

Introduction

Conclusions

References

Tables

Figures

◀

▶

◀

▶

Back

Close

Full Screen / Esc

Printer-friendly Version

Interactive Discussion



TransCom N₂O model inter-comparison

R. L. Thompson et al.

Table 3. Prior flux model overview (totals shown for 2005).

Category	Dataset	Resolution	Total (TgNyr ⁻¹)
terrestrial biosphere	ORCHIDEE O-CN	monthly	10.83
ocean	PISCES	monthly	4.28
waste water	EDGAR-4.1	annual	0.21
solid waste	EDGAR-4.1	annual	0.004
solvents	EDGAR-4.1	annual	0.05
fuel production	EDGAR-4.1	annual	0.003
ground transport	EDGAR-4.1	annual	0.18
industry combustion	EDGAR-4.1	annual	0.41
residential & other combustion	EDGAR-4.1	annual	0.18
shipping	EDGAR-4.1	annual	0.002
other sources	EDGAR-4.1	annual	0.0005
biomass burning	GFED-2	monthly	0.71
Total		monthly	16.84

Title Page

Abstract

Introduction

Conclusions

References

Tables

Figures

◀

▶

◀

▶

Back

Close

Full Screen / Esc

Printer-friendly Version

Interactive Discussion



TransCom N₂O model
inter-comparison

R. L. Thompson et al.

Title Page

Abstract

Introduction

Conclusions

References

Tables

Figures

◀

▶

◀

▶

Back

Close

Full Screen / Esc

Printer-friendly Version

Interactive Discussion

**Table 4.** Atmospheric observation sites using in the inversions. (F = Flask, C = Continuous).
Altitude is specified as metres above sea-level (m a.s.l.).

ID	Station	Operator	Type	Latitude	Longitude	Altitude (m a.s.l.)
ALT	Alert, Canada	NOAA	F	82.5° N	62.5° W	210
ASC	Ascension Isl., UK	NOAA	F	7.9° S	14.4° W	54
ASK	Assekrem, Algeria	NOAA	F	23.2° N	5.4° E	2728
AZR	Azores, Portugal	NOAA	F	38.8° N	27.4° W	40
BAL	Baltic Sea, Poland	NOAA	F	55.4° N	17.2° E	7
BIK	Bialystok, Poland	MPI-BGC	C	55.3° N	22.8° E	460
BKT	Bukit Kototabang, Indonesia	NOAA	F	0.2° S	100.3° E	865
BME	St. Davis Head, Bermuda, UK	NOAA	F	32.4° N	64.7° W	30
BMW	Tudor Hill, Bermuda, UK	NOAA	F	32.3° N	64.9° W	30
BRW	Barrow, Alaska	NOAA	F	71.3° N	156.6° W	11
BSC	Black Sea, Romania	NOAA	F	44.2° N	28.7° E	3
CBA	Cold Bay, Alaska	NOAA	F	55.2° N	162.7° W	21
CBW	Cabauw, Netherlands	ECN	C	52.0° N	4.9° E	118
CGO	Cape Grim, Tasmania	AGAGE	C	40.7° S	144.7° E	164
CHR	Christmas Isl.	NOAA	F	1.7° N	157.2° W	3
COI	Cape Ochi-ishi, Japan	NIES	C	43.2° N	145.5° E	45
CRZ	Crozet Isl., France	NOAA	F	46.45° S	51.9° E	120
CVR	Calhau, Cape Verde	MPI-BGC	F	16.9° N	24.9° W	10
EIC	Easter Island, Chile	NOAA	F	27.2° S	109.5° W	50
GMI	Mariana Isl., Guam	NOAA	F	13.4° N	144.8° E	2
HAT	Hateruma, Japan	NIES	C	24.1° N	123.8° E	10
HBA	Halley Stn., Antarctica	NOAA	F	75.6° S	26.5° W	30
HUN	Hegyhatsal, Hungary	ELTE	C	46.9° N	16.7° E	344
ICE	Heimay, Iceland	NOAA	F	63.3° N	20.3° W	118
IZO	Tenerife, Spain	NOAA	F	28.3° N	16.5° W	2360
JFJ	Jungfrauoch, Switzerland	EMPA	C	46.6° N	8.0° E	3580
KEY	Key Biscayne, Florida	NOAA	F	25.7° N	80.2° W	3
KUM	Cape Kumukahi	NOAA	F	19.5° N	154.8° W	3
KZD	Sary Tauku, Kazakhstan	NOAA	F	44.1° N	76.8° E	601

Table 4. Continued.

ID	Station	Operator	Type	Latitude	Longitude	Altitude (m a.s.l.)
LEF	Park Falls, Wisconsin	NOAA	F	45.9° N	90.3° W	868
LLN	Lulin, Taiwan	NOAA	F	23.5° N	120.9° E	2867
LUT	Lutjewad, Netherlands	RUG-CIO	C	53.4° N	6.4° E	60
MHD	Macehead, Ireland	AGAGE	C	53.3° N	9.9° W	25
MLO	Mauna Loa, Hawaii	NOAA	F	19.5° N	155.6° W	3397
NWR	Niwot Ridge	NOAA	F	40.0° N	105.5° W	3526
NMB	Gobabeb, Namibia	NOAA	F	23.6° S	15.0° E	456
OXK	Ochsenkopf, Germany	MPI-BGC	C	50.1° N	11.8° E	1185
PAL	Pallas, Finland	FMI	C	68.0° N	24.1° W	560
PSA	Palmer Stn, Antarctica	NOAA	F	64.9° S	64.0° W	10
PTA	Point Arena, California	NOAA	F	39.0° N	123.7° W	55
RPB	Ragged Point, Barbados	AGAGE	C	13.2° N	59.4° W	45
SEY	Mahe, Seychelles	NOAA	F	4.7° S	55.2° E	3
SHM	Shemya Isl., Alaska	NOAA	F	52.7° N	174.1° E	40
SIS	Shetland Isl., UK	MPI-BGC	F	59.9° N	1.3° W	46
SSL	Schauinsland	UBA	C	47.9° N	7.9° E	1205
SMO	Tutuila, American Samoa	AGAGE	C	14.3° S	170.6° W	42
SPO	South Pole, Antarctica	NOAA	F	89.98° S	24.8° W	2810
STM	ocean stn. M, Norway	NOAA	F	66.0° N	2.0° E	7
SUM	Summit, Greenland	NOAA	F	72.6° N	38.5° W	3238
SYO	Syowa Stn., Antarctica	NOAA	F	69.0° S	39.6° E	11
TAP	Tae-ahn Peninsula, Taiwan	NOAA	F	36.7° N	126.1° E	20
TDF	Tierra del Fuego, Argentina	NOAA	F	54.9° S	68.5° W	20
THD	Trinidad Head, California	AGAGE	C	41.1° N	124.2° W	107
TTA	Griffin, UK	UEDIN	C	56.6° N	3.0° W	535
UTA	Wendover, Utah	NOAA	F	39.9° N	113.7° W	132
UUM	Ulaan Uul, Mongolia	NOAA	F	44.5° N	111.1° E	914
WIS	Negev Desert, Israel	NOAA	F	31.1° N	34.9° E	400
WKT	Moody, Texas	NOAA	F	31.3° N	97.3° W	708
WLG	Mt. Waliguan, China	NOAA	F	36.3° N	100.9° E	3810
ZEP	Ny-Alesund	NOAA	F	78.9° N	11.88° E	475
ZOT	Zotto, Russia	MPI-BGC	F	60.8° N	89.4° E	415

**TransCom N₂O model
inter-comparison**

R. L. Thompson et al.

Title Page

Abstract Introduction

Conclusions References

Tables Figures

◀ ▶

◀ ▶

Back Close

Full Screen / Esc

Printer-friendly Version

Interactive Discussion



TransCom N₂O model
inter-comparison

R. L. Thompson et al.

Table 5. A priori and a posteriori calibration offsets (ppb) relative to the NOAA2006A scale. Note that only LMDZ4 and TM5 included the optimization of calibration offsets and only TM5 calculated these annually (the range over all years is given in brackets for TM5).

ID	Prior	TM5	LMDZ4	ID	Prior	TM5	LMDZ4
BIK	0.06	0.22 (0.00–0.47)	0.13	PAL	0.50	0.00 (0.0–0.0)	0.32
CBW	0.27	0.52 (0.25–0.76)	0.84	MHD	0.25	0.08 (0.25–0.76)	0.05
HUN	1.08	0.45 (0.24–0.59)	0.44	THD	–0.30	0.04 (–0.01–0.07)	0.28
LUT	–3.0	–1.2 (–2.0–0.0)	–2.0	RPB	0.00	–0.11 (–0.21–0.0)	0.07
OXK	0.39	0.77 (0.0–1.28)	1.13	SMO	0.20	0.24 (0.14–0.37)	0.36
TTA	0.00	0.56 (0.0–1.03)	0.65	CGO	0.20	0.08 (0.0–0.13)	0.00
JFJ	0.00	–0.47 (–0.69––0.34)	–0.60	NIES	–0.60	0.00 (0.0–0.0)	–0.41
SSL	0.00	0.30 (0.07–0.50)	0.17	MPI-BGC	0.00	0.38 (0.19–0.54)	0.47

Title Page

Abstract

Introduction

Conclusions

References

Tables

Figures

◀

▶

◀

▶

Back

Close

Full Screen / Esc

Printer-friendly Version

Interactive Discussion



TransCom N₂O model inter-comparison

R. L. Thompson et al.

Table 6. Overview of the prior and posterior global annual total source (upper panel) and sink (lower panel) (both in TgNyr⁻¹).

Year	Prior	MOZART4	ACTMt42I67	TM5	TM3	LMDZ4
2006	16.3	14.1	16.0	16.9	15.1	17.6
2007	16.8	15.6	16.7	16.9	16.6	19.1
2008	16.2	15.7	16.5	17.2	16.4	19.4
2009	16.4	14.4	15.5	15.4	15.6	18.8
2006	–	12.8	11.9	12.2	12.4	12.7
2007	–	12.6	12.4	12.6	12.4	12.7
2008	–	12.6	12.5	12.4	12.5	12.5
2009	–	12.7	13.0	12.4	12.6	12.7

[Title Page](#)
[Abstract](#)
[Introduction](#)
[Conclusions](#)
[References](#)
[Tables](#)
[Figures](#)
[◀](#)
[▶](#)
[◀](#)
[▶](#)
[Back](#)
[Close](#)
[Full Screen / Esc](#)
[Printer-friendly Version](#)
[Interactive Discussion](#)


TransCom N₂O model inter-comparison

R. L. Thompson et al.

Table 7. Annual mean (2006–2008) regional N₂O emission estimates (TgNyr⁻¹). Values for which the inversions differ on the direction of the change with respect to the prior are shown in brackets. (MAD = Median Absolute Deviation).

Region	Prior	Posterior		
		Range	Median	MAD
ocean 90–30° S	1.49	0.92–1.34	1.08	0.20
ocean 30° S–30° N	3.30	3.25–3.69	(3.66)	0.03
ocean 30–90° N	0.95	1.13–1.29	1.20	0.08
S + Tr America	2.55	1.99–2.62	(2.33)	0.27
N America	1.00	0.65–1.29	(0.74)	0.11
Africa	3.07	3.23–3.40	3.36	0.04
Europe	0.80	0.84–1.20	1.04	0.20
N Asia	0.40	0.31–0.67	(0.40)	0.09
S Asia	2.91	2.56–3.81	(2.85)	0.28
Australasia	0.39	0.27–0.36	0.31	0.01

[Title Page](#)
[Abstract](#)
[Introduction](#)
[Conclusions](#)
[References](#)
[Tables](#)
[Figures](#)
[I◀](#)
[▶I](#)
[◀](#)
[▶](#)
[Back](#)
[Close](#)
[Full Screen / Esc](#)
[Printer-friendly Version](#)
[Interactive Discussion](#)


TransCom N₂O model
inter-comparison

R. L. Thompson et al.

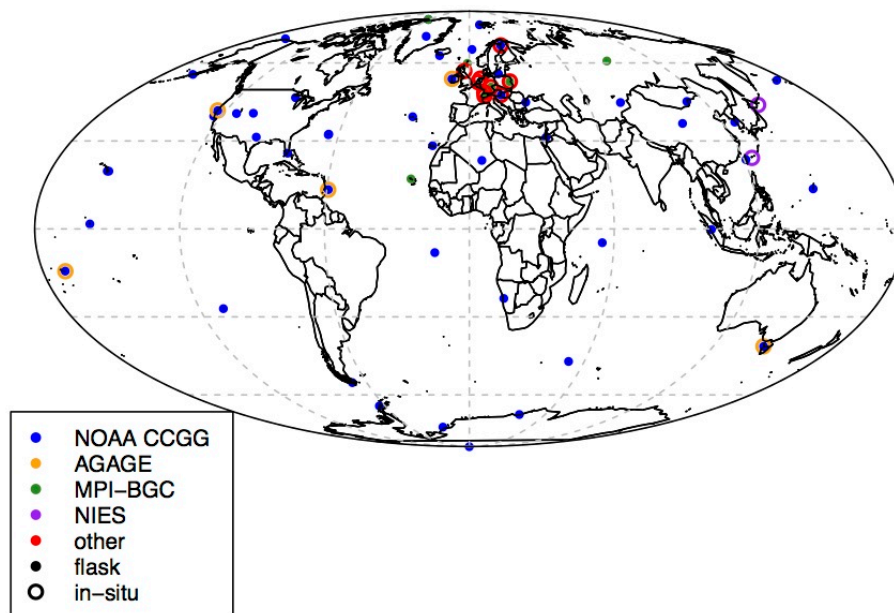


Fig. 1. Map of surface sites for atmospheric observations.

[Title Page](#)[Abstract](#)[Introduction](#)[Conclusions](#)[References](#)[Tables](#)[Figures](#)[◀](#)[▶](#)[◀](#)[▶](#)[Back](#)[Close](#)[Full Screen / Esc](#)[Printer-friendly Version](#)[Interactive Discussion](#)

TransCom N₂O model
inter-comparison

R. L. Thompson et al.

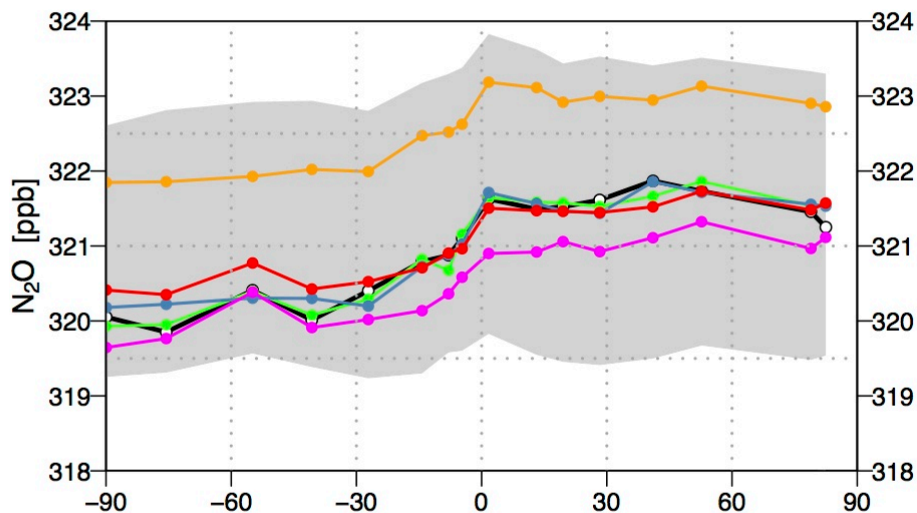


Fig. 2. Comparison of the annual mean N₂O gradient (ppb) for 2006 to 2009 with surface observations. The grey shaded area shows the range of values for the model using the prior fluxes. (Legend: observations, black; MOZART4, orange; ACTMt42l67, green; TM5, blue; TM3, red; LMDZ4, magenta.)

[Title Page](#)[Abstract](#)[Introduction](#)[Conclusions](#)[References](#)[Tables](#)[Figures](#)[◀](#)[▶](#)[◀](#)[▶](#)[Back](#)[Close](#)[Full Screen / Esc](#)[Printer-friendly Version](#)[Interactive Discussion](#)

TransCom N₂O model inter-comparison

R. L. Thompson et al.

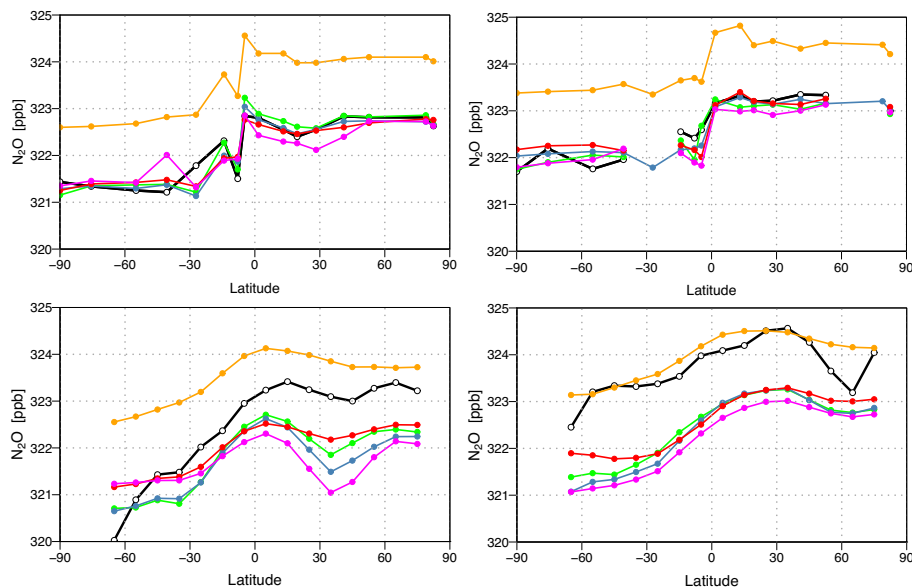


Fig. 3. Comparison of model simulations with observations of N₂O mole fraction (ppb) from surface sites (upper) and pressure-weighted column averages (up to 10 000 m) from HIPPO aircraft profiles (lower) for January (left) and November (right) 2009. (Legend: observations, black; MOZART4, orange; ACTMt42I67, green; TM5, blue; TM3, red; LMDZ4, magenta.)

Title Page

Abstract

Introduction

Conclusions

References

Tables

Figures

◀

▶

◀

▶

Back

Close

Full Screen / Esc

Printer-friendly Version

Interactive Discussion



TransCom N₂O model
inter-comparison

R. L. Thompson et al.

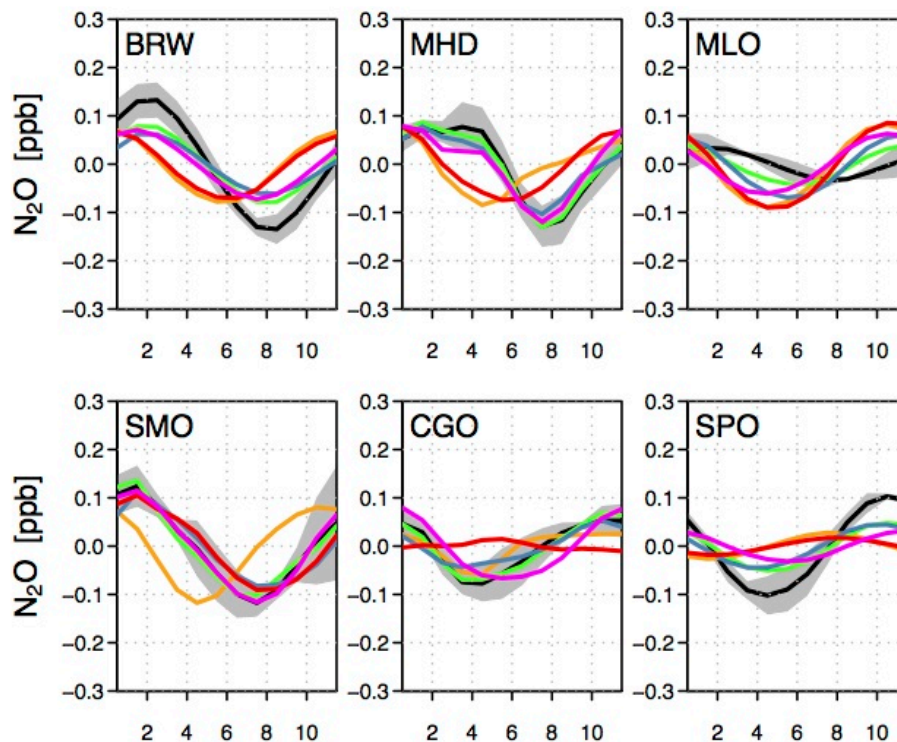


Fig. 4. Comparison of the mean (2006–2008) observed and simulated seasonal cycles in N₂O mole fraction (ppb) at selected key sites. The grey shaded indicates the range of uncertainty (1σ standard deviation) in the observations. For a description of the site abbreviations see Table 4. (Legend: observations, black; MOZART4, orange; ACTMt42I67, green; TM5, blue; TM3, red; LMDZ4, magenta.)

Title Page

Abstract

Introduction

Conclusions

References

Tables

Figures

◀

▶

◀

▶

Back

Close

Full Screen / Esc

Printer-friendly Version

Interactive Discussion



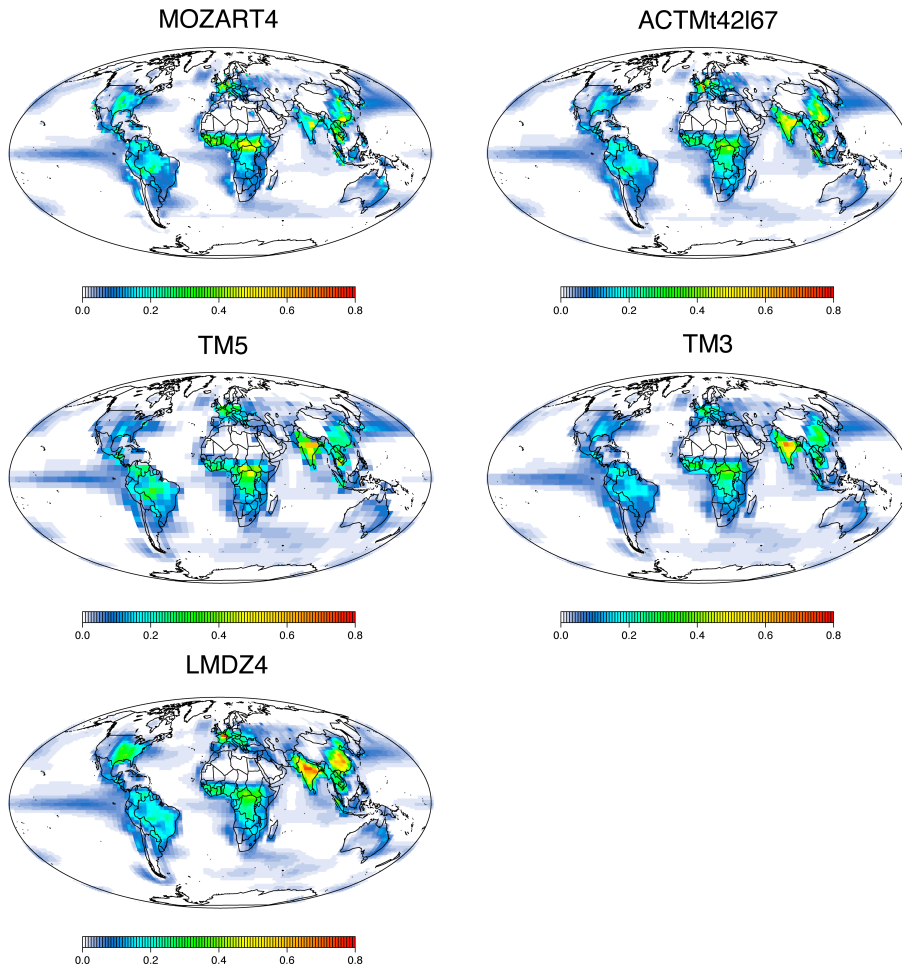


Fig. 5. Maps of annual mean posterior N_2O flux ($\text{gNm}^{-2}\text{yr}^{-1}$) for 2006–2008.

Title Page	
Abstract	Introduction
Conclusions	References
Tables	Figures
◀	▶
◀	▶
Back	Close
Full Screen / Esc	
Printer-friendly Version	
Interactive Discussion	



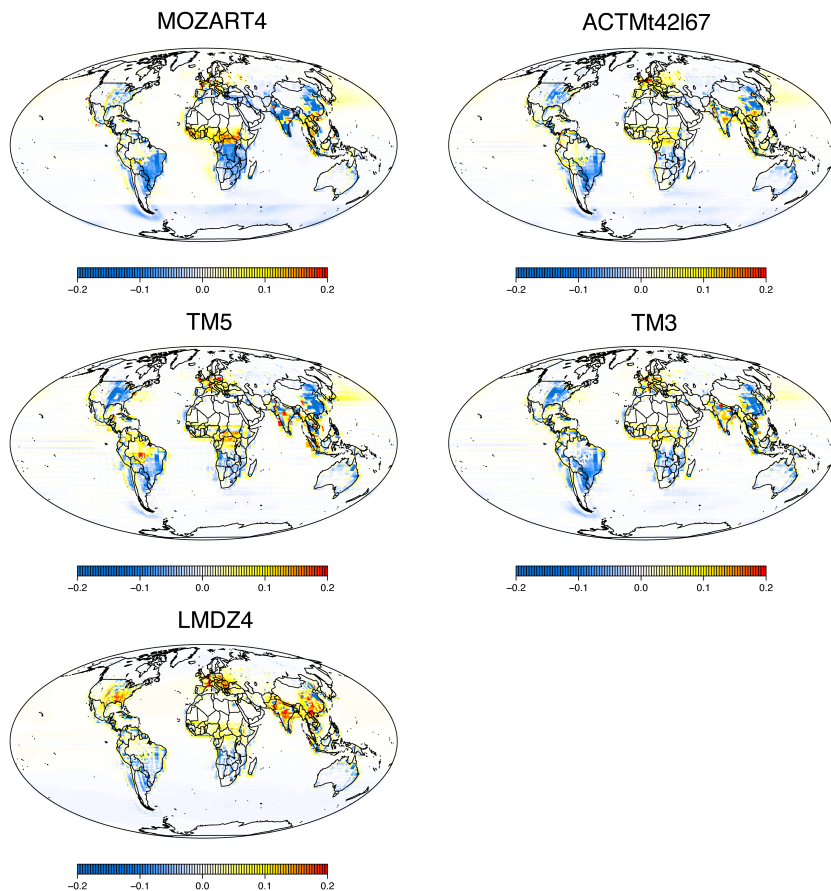


Fig. 6. Maps of annual mean flux increments for 2006–2008 ($\text{gN m}^{-2} \text{yr}^{-1}$) relative to the prior fluxes.

Title Page

Abstract

Introduction

Conclusions

References

Tables

Figures

◀

▶

◀

▶

Back

Close

Full Screen / Esc

Printer-friendly Version

Interactive Discussion



TransCom N₂O model
inter-comparison

R. L. Thompson et al.

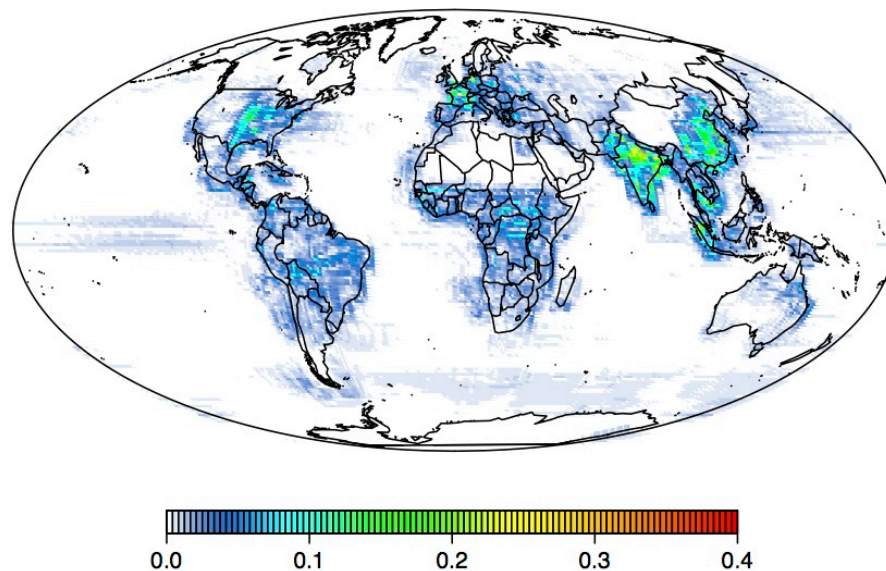


Fig. 7. Map of median absolute deviation (MAD) of annual mean fluxes (gNm⁻²yr⁻¹).

[Title Page](#)[Abstract](#)[Introduction](#)[Conclusions](#)[References](#)[Tables](#)[Figures](#)[◀](#)[▶](#)[◀](#)[▶](#)[Back](#)[Close](#)[Full Screen / Esc](#)[Printer-friendly Version](#)[Interactive Discussion](#)

TransCom N₂O model
inter-comparison

R. L. Thompson et al.

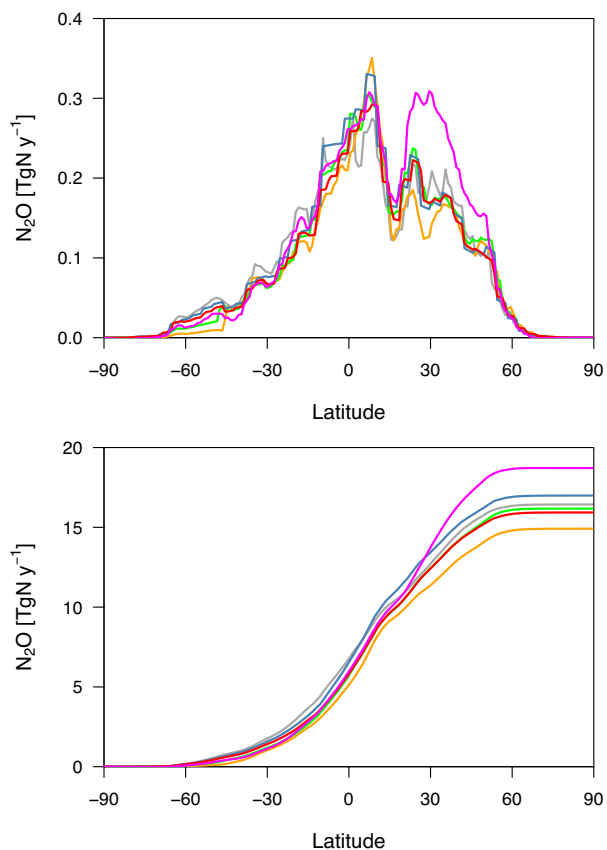


Fig. 8. Zonally integrated annual mean (2006–2008) fluxes (top) and accumulated from south to north (bottom). (Legend: prior, grey; MOZART4, orange; ACTMt42I67, green; TM5, blue; TM3, red; LMDZ4, magenta.)

[Title Page](#)[Abstract](#)[Introduction](#)[Conclusions](#)[References](#)[Tables](#)[Figures](#)[◀](#)[▶](#)[◀](#)[▶](#)[Back](#)[Close](#)[Full Screen / Esc](#)[Printer-friendly Version](#)[Interactive Discussion](#)

TransCom N₂O model inter-comparison

R. L. Thompson et al.

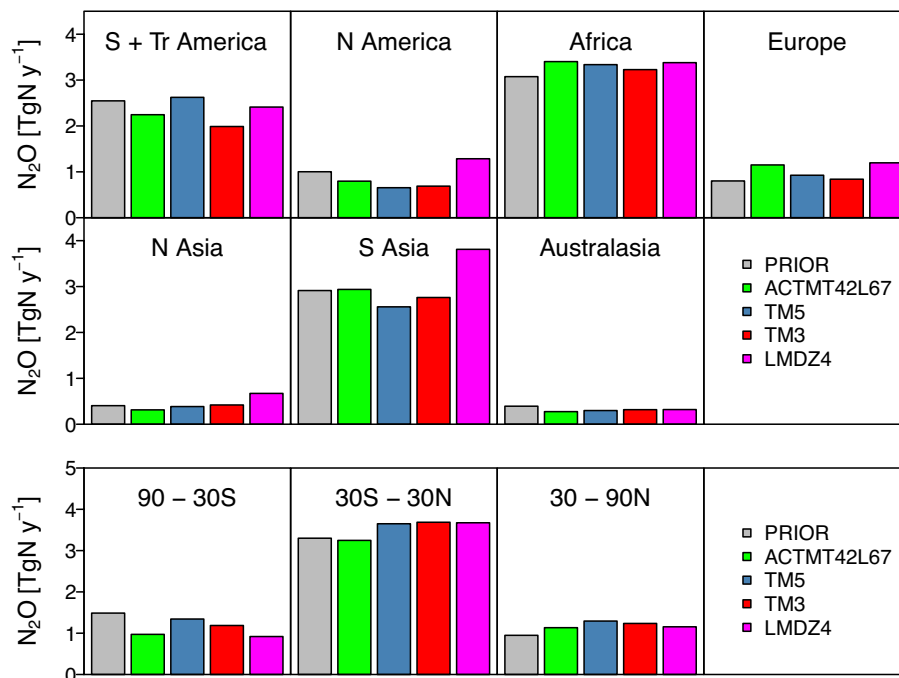


Fig. 9. Annual mean (2006–2008) regional emission estimates (TgNyr⁻¹) for the 7 land and 3 ocean regions. The colours refer to the different inversion frameworks as indicated in the legend.

Title Page

Abstract

Introduction

Conclusions

References

Tables

Figures

◀

▶

◀

▶

Back

Close

Full Screen / Esc

Printer-friendly Version

Interactive Discussion



TransCom N₂O model inter-comparison

R. L. Thompson et al.

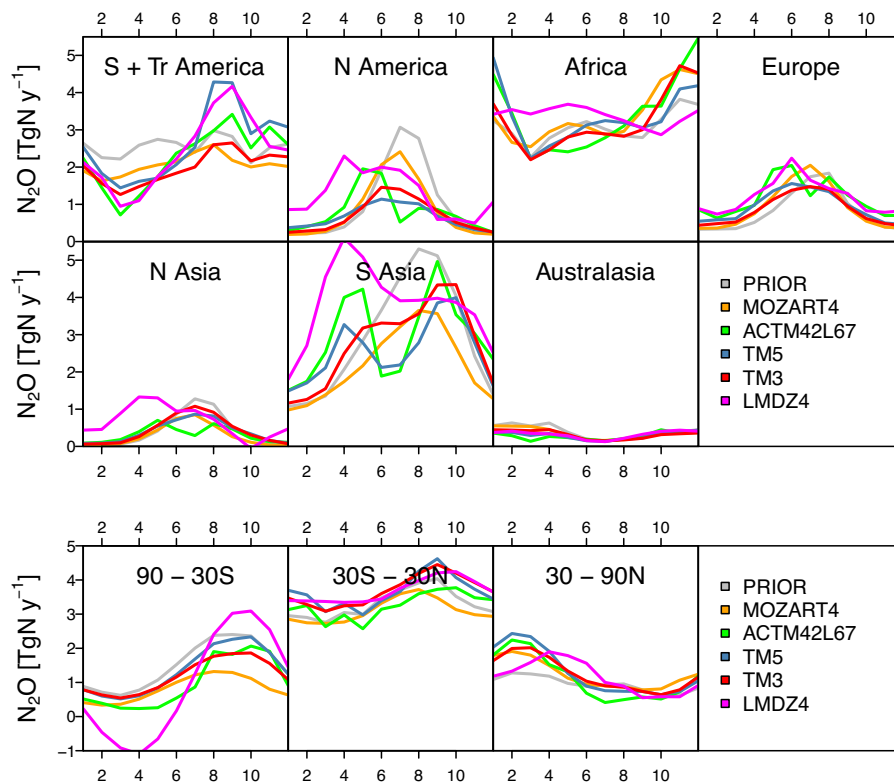


Fig. 10. Mean (2006–2008) seasonal cycle in N₂O flux (TgNyr⁻¹) for each of the 7 sub-continental and 3 ocean regions.

Title Page

Abstract Introduction

Conclusions References

Tables Figures

◀ ▶

◀ ▶

Back Close

Full Screen / Esc

Printer-friendly Version

Interactive Discussion



TransCom N₂O model inter-comparison

R. L. Thompson et al.

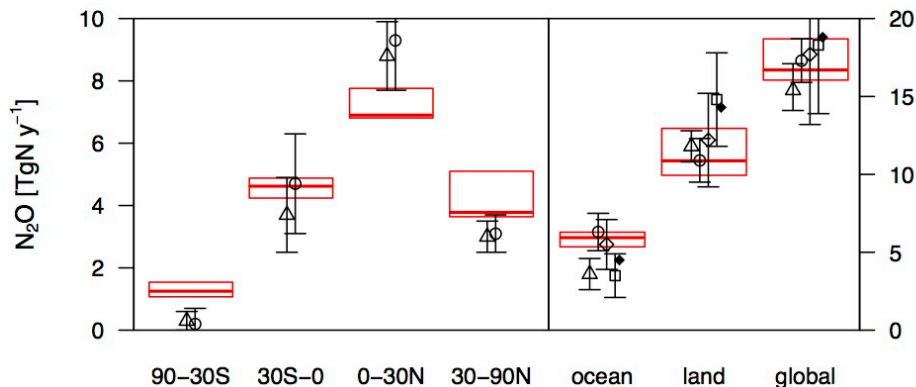


Fig. 11. Comparison of the total emissions for each semi-hemisphere region, the ocean, land and globally from this study with previous estimates. The vertical extents of the red boxes indicate the range and the horizontal lines in the interior indicate the median of inversion estimates from this study. The points indicate the values from previous studies: Hirsch et al. (2006), open circles; Huang et al. (2008), triangles; AR4, diamonds; Syakila et al. (2011), solid circles; Zaehle et al. (2011), squares. The error bars indicate the 1σ uncertainty.

Title Page

Abstract

Introduction

Conclusions

References

Tables

Figures

◀

▶

◀

▶

Back

Close

Full Screen / Esc

Printer-friendly Version

Interactive Discussion



TransCom N₂O model
inter-comparison

R. L. Thompson et al.

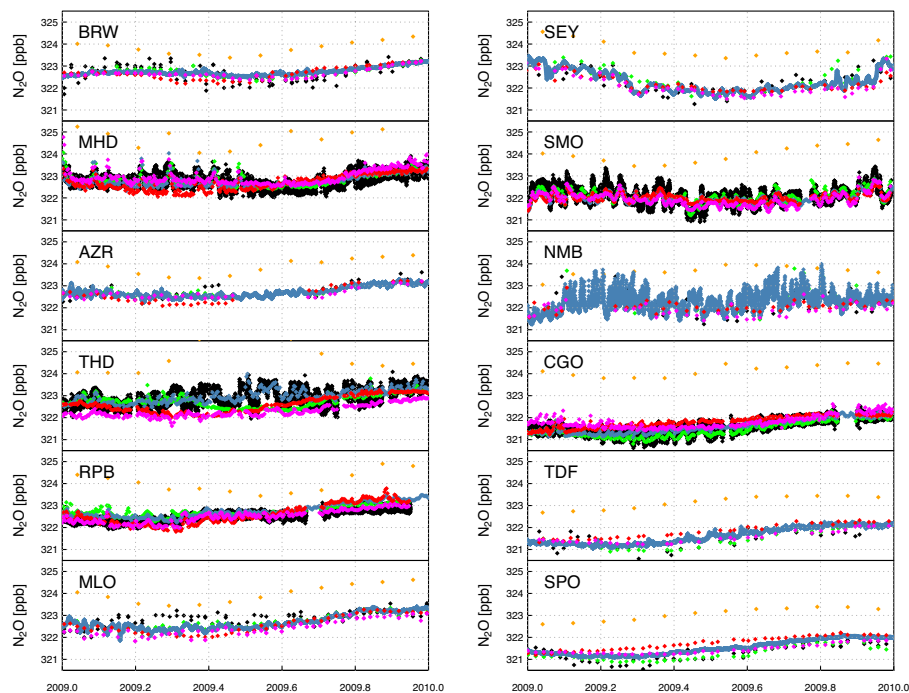


Fig. A1. Comparison of the daily mean N₂O mole fractions (ppb) simulated by integrating the CTMs with their corresponding posterior fluxes. Note for MOZART4 only monthly means were submitted. (Legend: observations, black; MOZART4, orange; ACTMt42I67, green; TM5, blue; TM3, red; LMDZ4, magenta.)

Title Page

Abstract

Introduction

Conclusions

References

Tables

Figures

◀

▶

◀

▶

Back

Close

Full Screen / Esc

Printer-friendly Version

Interactive Discussion



TransCom N₂O model
inter-comparison

R. L. Thompson et al.

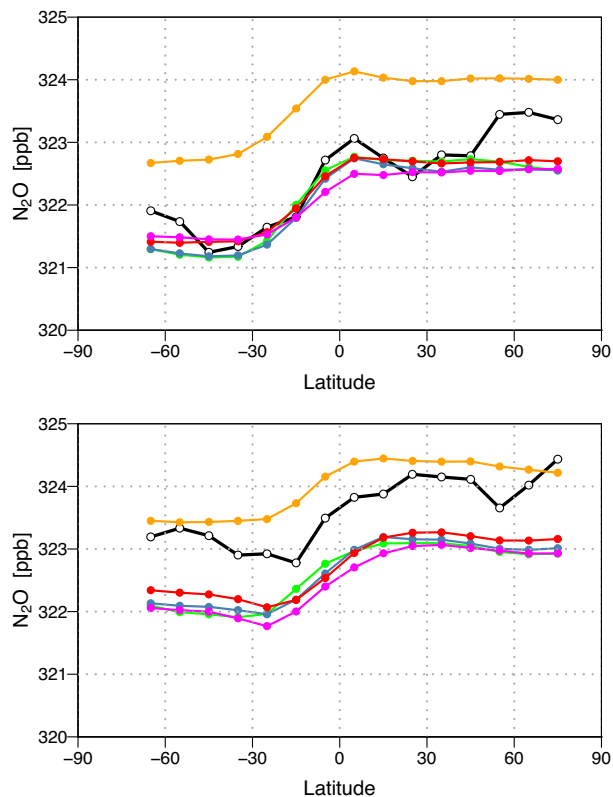


Fig. A2. Comparison of model simulations with pressure-weighted column averages from HIPPO aircraft profiles for January (top) and November (bottom) 2009. The column average was calculated from the surface up to 2000 m. (Legend: observations, black; MOZART4, orange; ACTMt42l67, green; TM5, blue; TM3, red; LMDZ4, magenta.)

[Title Page](#)[Abstract](#)[Introduction](#)[Conclusions](#)[References](#)[Tables](#)[Figures](#)[◀](#)[▶](#)[◀](#)[▶](#)[Back](#)[Close](#)[Full Screen / Esc](#)[Printer-friendly Version](#)[Interactive Discussion](#)

TransCom N₂O model
inter-comparison

R. L. Thompson et al.

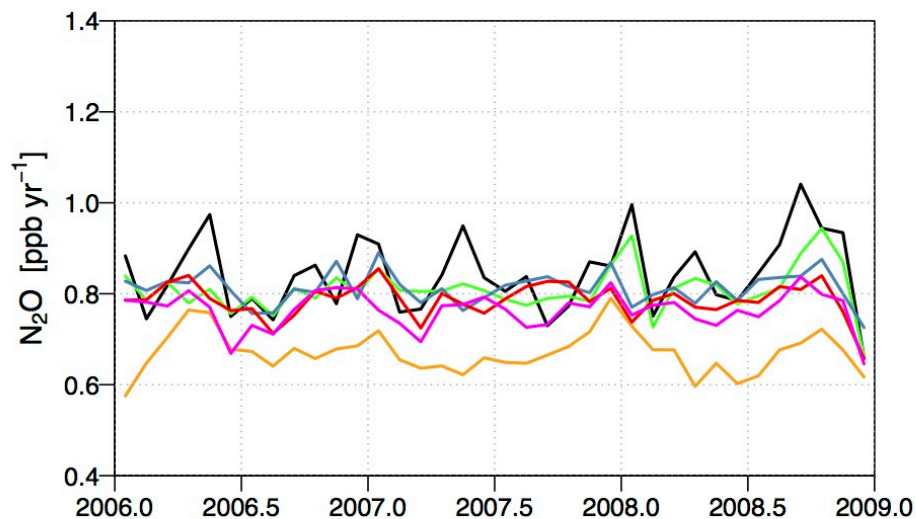


Fig. A3. Growth rate in atmospheric N₂O mole fraction (ppb yr⁻¹). (Legend: observations, black; MOZART4, orange; ACTMt42I67, green; TM5, blue; TM3, red; LMDZ4, magenta.)

[Title Page](#)[Abstract](#)[Introduction](#)[Conclusions](#)[References](#)[Tables](#)[Figures](#)[◀](#)[▶](#)[◀](#)[▶](#)[Back](#)[Close](#)[Full Screen / Esc](#)[Printer-friendly Version](#)[Interactive Discussion](#)

TransCom N₂O model
inter-comparison

R. L. Thompson et al.

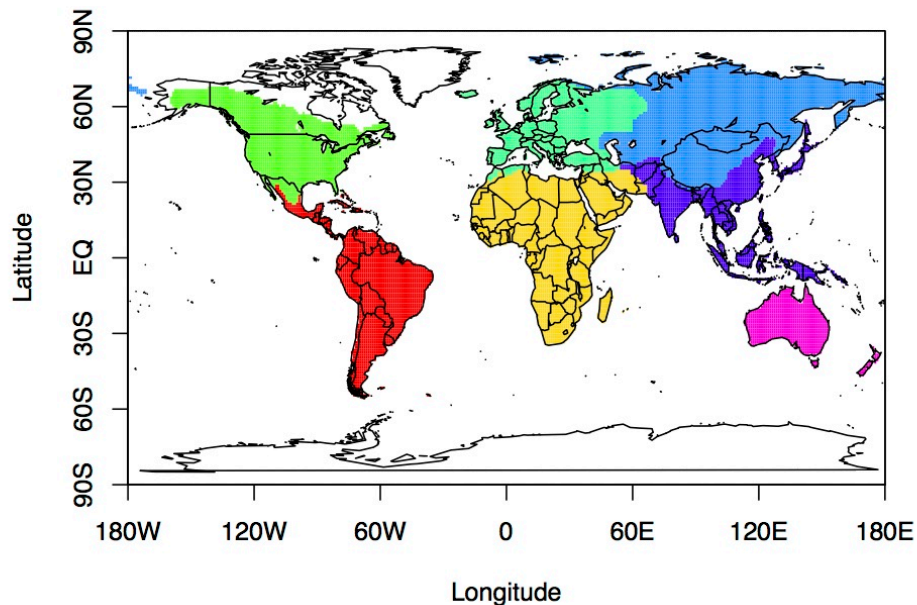


Fig. A4. Map of the 7 sub-continental regions used in the analysis. (North America = green, Tropical & South America = red, Africa = yellow, Europe = cyan, North Asia = blue, South Asia = purple, Australasia = magenta.)

[Title Page](#)[Abstract](#)[Introduction](#)[Conclusions](#)[References](#)[Tables](#)[Figures](#)[◀](#)[▶](#)[◀](#)[▶](#)[Back](#)[Close](#)[Full Screen / Esc](#)[Printer-friendly Version](#)[Interactive Discussion](#)